Supporting Information

Understanding and designing one-dimensional assemblies of ligand-protected metal nanoclusters

Sakiat Hossain,[a] Yukari Imai,[a] Yuichi Motohashi,[b,c] Zhaoheng Chen,[a] Daiki Suzuki,[a] Taiyo Suzuki,[a] Yuki Kataoka,[a] Momoko Hirata,[a] Tasuku Ono,[a] Wataru Kurashige,[a] Tokuhisa Kawawaki,[a,d] Takahiro Yamamoto,[c,d] and Yuichi Negishi,[*,a,d]

[a]*Department of Applied Chemistry, Faculty of Science, Tokyo University of Science, Kagurazaka, Shinjuku−ku, Tokyo 162−8601, Japan*
[b]*Ricoh Company, Ltd., Izumi−ku, Ebina, Kanagawa 243−0460, Japan*
[c]*Department of Liberal Arts, Faculty of Engineering, Tokyo University of Science, Katsushika−ku, Tokyo 125−8585, Japan*
[d]*Research Institute for Science & Technology, Tokyo University of Science, Shinjuku−ku, Tokyo 162−8601, Japan*

Corresponding Author E-mail: negishi@rs.kagu.tus.ac.jp (Y. Negishi)

1. Experimental Section

1.1. Chemicals

All the chemicals used in this study were commercially obtained and used without further purification. Hydrogen tetrachloroaurate tetrahydrate ($HAuCl_4 \cdot 4H_2O$) and hydrogen hexachloroplatinate hexahydrate ($H_2PtCl_6 \cdot 6H_2O$) were purchased from Tanaka Kikinzoku. Tetraoctylammonium bromide ($(C_8H_{17})_4NBr$), dichloromethane, 2-phenylethanethiol (PhC_2H_4SH), silica gel (spherical, 63-210 μm), 1-propanethiol (C_3H_7SH), 2,4,6-trimethylbenzylmercaptane ($(CH_3)_3PhCH_2SH$) and ethyl mercaptane (C_2H_5SH) were obtained from FUJIFILM Wako Pure Chemical Co.. Sodium hydroborate ($NaBH_4$), *trans*-2-[3-(4-*tert*-butylphenyl)-2-methyl-2-propenylidene]malononitrile (DCTB), 2-chlorobenzylmercaptane ($ClPhCH_2SH$), isopropanethiol ($(CH_3)_2CHSH$), 4-*tert*-butylbenzylmercaptane (^{t}BuPhCH_2SH), 4-*tert*-butylbenzenethiol (^{t}BuPhSH), benzyl mercaptane ($PhCH_2SH$) and isobuthyl mercaptane ($(CH_3)_2C_2H_3SH$) were sourced from Tokyo Chemical Industry. Tetrahydrofuran (THF), ethanol, methanol, toluene and hexane were obtained from Kanto Chemical Co., Inc.. Cesium acetate (CH3COOCs) was from Nacalai Tesque. Pure Milli-Q water (H_2O; 18.2 MΩ·cm) was generated using a Merck Millipore Direct 3 UV system.

1.2. Synthesis and Crystallization

$[Au_4Pt_2(SCH(CH_3)_2)_8]^0$ (a) 164.5 mg (0.40 mmol) of $HAuCl_4 \cdot 4H_2O$, 22.5 mg (0.10 mmol) of $H_2PtCl_6 \cdot 6H_2O$, and 317 mg (0.58 mmol) of $(C_8H_{17})_4NBr$ was dissolved in 15 mL of THF. After 30 min of stirring, 100 mg (1.3 mmol) of $(CH_3)_2CHSH$ was added to the solution. After 45 min of stirring, 6 mL of ice water containing 190 mg (5.0 mmol) of $NaBH_4$ was added to the solution. This reaction was continued for 12 h under strong stirring at room temperature. After the reaction, THF was removed by rotary evaporator. Excess $NaBH_4$ was removed by 1−2 times of water wash and also by a mixture of H_2O:methanol = 1:2 once. After that, the product was extracted by methanol. Excess $(CH_3)_2CHSH$ was removed by vacuum line over 12 h until the smell of $(CH_3)_2CHSH$ was completely removed. Then, the expected sample was separated from brown color sample containing large clusters by GPC. After GPC, the product was purified by an open column that was loaded with silica gel and a mixture of solvent (dichloromethane:hexane = 1:19) was used as starting eluent solvent and gradually eluent's polarity was increased (dichloromethane:hexane = 1:4). The first fraction was collected. Crystal was grown by vapor diffusion (Figure S4). THF was used as good solvent and methanol was used as poor solvent.

[Au$_4$Pt$_2$(SCH$_2$Ph(CH$_3$)$_3$)$_8$]^0 (b) 164.5 mg (0.40 mmol) of $HAuCl_4 \cdot 4H_2O$, 22.5 mg (0.10 mmol) of $H_2PtCl_6 \cdot 6H_2O$, and 317 mg (0.58 mmol) of $(C_8H_{17})_4NBr$ was dissolved in 15 mL of THF. After stirring of 30 min, 433 mg (2.6 mmol) of $(CH_3)_3PhCH_2SH$ was added to the solution. After 2 h of reaction at room temperature, methanol was added in the reaction system to remove excess $(CH_3)_3PhCH_2SH$. When methanol was added, precipitation was confirmed. This process was continued at least 3 times. After that, the product was extracted by toluene. Crystals was grown by vapor diffusion (Figure S4). Toluene was used as good solvent and methanol was used as poor solvent.

[Au$_4$Pt$_2$(SCH$_2$Ph^{t}Bu)$_8$]^0 (c) 164.5 mg (0.40 mmol) of $HAuCl_4 \cdot 4H_2O$, 22.5 mg (0.10 mmol) of $H_2PtCl_6 \cdot 6H_2O$, and 317 mg (0.58 mmol) of $(C_8H_{17})_4NBr$ was dissolved in 15 mL of THF. After 30 min of stirring, 468 mg (2.6 mmol) of ^{t}BuPhCH$_2$SH was added to the solution. After 45 min of stirring, 6 mL of ice water containing 190 mg (5.0 mmol) of $NaBH_4$ was added to the solution. This reaction was continued for 5 h under strong stirring at room temperature. Excess $NaBH_4$ was removed by 1−2 times of water wash. Excess ^{t}BuPhCH$_2$SH was removed by methanol wash at least 3 times. After that, the product was extracted by toluene. Expected product was separated by two times of GPC. In first time GPC, the second fraction was collected (first fraction, which included the large cluster, was removed) and in second time GPC, only the top of the first fraction was collected. Crystals was grown by vapor diffusion (Figure S4). Toluene was used as good solvent and ethanol was used as poor solvent.

[Au$_4$Pt$_2$(SCH$_2$PhCl)$_8$]^0 (d) 164.5 mg (0.40 mmol) of $HAuCl_4 \cdot 4H_2O$, 22.5 mg (0.10 mmol) of $H_2PtCl_6 \cdot 6H_2O$, and 317 mg (0.58 mmol) of $(C_8H_{17})_4NBr$ was dissolved in 15 mL of THF. After 30 mins stirring, 413 mg (2.6 mmol) of ClPhCH$_2$SH was added to the solution. After 1 h of stirring, 6 mL of ice water containing 190 mg (5.0 mmol) of $NaBH_4$ was added to solution. This reaction was continued for 1 h under strong stirring at room temperature. Excess $NaBH_4$ was removed by 1−2 times of water wash. Excess ClPhCH$_2$SH was removed by methanol wash at least 3 times. After that, product was extracted by toluene. After the complete removal of ClPhCH$_2$SH, the product was separated by gel permeation chromatography (GPC) and second peak from light side was collected. After GPC, the product was purified by an open column that was loaded with silica gel and a mixture of solvent (dichloromethane:hexane = 1:19) as starting eluent and slowly solvent polarity was increased (maximum 1:4). The first fraction was collected. Crystals was grown by vapor diffusion (Figure S4). Toluene was used as good solvent and ethanol was used as poor solvent.

[Au$_4$Pt$_2$(SC$_2$H$_4$Ph)$_8$]^0 (e) 164.5 mg (0.40 mmol) of $HAuCl_4 \cdot 4H_2O$ and 22.5 mg (0.10 mmol) of $H_2PtCl_6 \cdot 6H_2O$, and 317 mg (0.58 mmol) of $(C_8H_{17})_4NBr$ was dissolved in 15 mL of THF. After 30 min of stirring, 180 μL (1.3 mmol) of PhC$_2$H$_4$SH was added to the solution. After 30 min of stirring, 6 mL of ice water containing 190 mg (5.0 mmol) of $NaBH_4$ was added to the solution. This reaction was continued for 3 h under strong stirring at room temperature. After reaction, THF was removed by rotary evaporator. Excess $NaBH_4$ was removed by 1−2 times of water wash. Excess PhC$_2$H$_4$SH was removed by methanol wash at least 3 times. Then, the product was extracted by toluene. The product was purified by an open column that was loaded with silica gel and a mixture of solvent (toluene:hexane = 3:2) as eluent, and the first fraction was collected. Crystal was got by vapor diffusion (Figure S4). Toluene was used as good solvent and ethanol was used as poor solvent.

[Au$_4$Pt$_2$(SC$_3$H$_7$)$_8$]^0 (f) 164.5 mg (0.40 mmol) of $HAuCl_4 \cdot 4H_2O$, 22.5 mg (0.10 mmol) of $H_2PtCl_6 \cdot 6H_2O$, and 317 mg (0.58 mmol) of $(C_8H_{17})_4NBr$ was dissolved in 15 mL of THF. After 30 min stirring, 118 μL (1.3 mmol) of C_3H_7SH was added to the solution. After 30 min of stirring, 6 mL of ice water containing 190 mg (5.0 mmol) of $NaBH_4$ was added to the solution. This reaction was continued for 5 h under strong stirring at room temperature. After reaction, THF was removed by rotary evaporator. Excess $NaBH_4$ was removed by 1−2 times

of water wash. Excess C_3H_7SH was removed by methanol wash at least 3 times. After that, the product was extracted by toluene. The product was purified by an open column that was loaded with silica gel and a mixture of solvent (dichloromethane:hexane = 1:19) as eluent at first time, after that increase the ratio slowly (maximum 1:4). The first fraction was collected. Crystal was got by vapor diffusion (Figure S4). Toluene was used as good solvent and ethanol was used as poor solvent.

Other $[Au_4Pt_2(SR)_8]^0$ $[Au_4Pt_2(SR)_8]^0$ was also synthesized using the other thiols as a ligand, such as benzyl mercaptan, isobutyl mercaptan, ethyl mercaptan, instead of the thiols listed in Scheme 2 (Figure S3). However, we could not grow the single crystal for these $[Au_4Pt_2(SR)_8]^0$.

1.3. Characterization

Matrix assisted laser desorption/ionization (MALDI) mass spectra were collected by a spiral time-of-flight mass spectrometer (JEOL, JMSS3000) with a semiconductor laser (λ = 349 nm). DCTB[1] was used as the MALDI matrix. To minimize dissociation of the cluster induced by laser irradiation, the cluster-to-matrix ratio was fixed to 1:1000.

Electrospray ionization (ESI) mass spectrometry was performed using a time-of-flight mass spectrometer (Bruker, micrOTOF II). In these measurements, a cluster solution with a concentration of 1 mg/mL in dichloromethane/methanol (1:1 = v:v) containing CH_3COOCs was electrosprayed at a flow rate of 1800 μL/h.

Diffraction data for the crystals (**b**−**e**) was collected on a SMART APEX 2 Ultra equipped with an Apex II CCD diffractometer whereas for crystal **a**, it was collected in a SMART APEX fitted with SMART APEX I CCD diffractometer. From the collected data, unit cell, integration, absorption correction (multi-scan), and space group (based on intensity statistics and systematic absences) were determined using the Bruker APEX 3 software package.[3] Crystal structures were solved by the intrinsic phasing method in APEX 3.[2] Final refinements were performed by SHELXL-2018/3[4] using the Olex 2 platform[5] (Table S7−S9).

X-ray photoelectron spectroscopy (XPS) analysis was performed using a JEOL JPS-9010MC electron spectrometer equipped with a chamber at a base pressure of ∼2×10^{-8} Torr. X-rays from the Mg Kα line (1253.6 eV) were used for excitation. Binding energies were corrected using the binding energy of C 1s (284.6 eV).

Optical absorption spectra of the cluster dichloromethane-solution, solid sample and crystal sample were obtained at room temperature with a spectrometer (JASCO, V-670). Solid sample was prepared by just drying the solution sample. Thus, the solid sample should be the amorphous film. In the measurements of the crystal sample, we used many crystals for one measurement.

1.4. Stability of Clusters

All the $[Au_4Pt_2(SR)_8]^0$ were stable in toluene solution. The formed crystals were also stable in toluene and in air. However, in dichloromethane solution, $[Au_4Pt_2(SC_2H_4Ph)_8]^0$ deteriorated gradually and the precipitate was formed after a long time. The formed precipitate was not dissolved in solvent.

2. Theoretical Section

The electronic structures of $[Au_4Pt_2(SC_2H_4Ph)_8]^0$ and $[Au_4Pt_2(SCH_2PhCl)_8]^0$ were calculated using first-principles calculations based on DFT. The ligand structures were optimized with gold, platinum and sulfur atoms fixed on the coordinates obtained by SCXRD (Figure 3). Calculations were performed using QuantumATK 2018.06 package,[6,7] which is a commercial software for atomic scale simulation based on DFT using atomic orbital basis sets. The generalized gradient approximation (GGA) was used with the Perdew-Burke-Ernzerhof (PBE) functional (GGA.PBE) and a mesh cut-off energy of 80 Hartree. Convergence is taken to have been achieved when the force on each atom reaches 0.01 eV/Å.

3. Additional Tables

Table S1. Synthesis Condition of a−f

cluster	thiol	[Au]:[Pt] [a]	Au/mmol [b]	thiol/mmol	$NaBH_4$/mmol	byproduct [c] (larger cluster)
a	$(CH_3)_2CHSH$	4:1	0.4	1.3	5.0	exist
b	$(CH_3)_3PhCH_2SH$	4:1	0.4	2.6	–	–
c	^{t}BuPhCH_2SH	4:1	0.4	2.6	5.0	exist
d	Cl$PhCH_2SH$	4:1	0.4	2.6	5.0	exist
e	PhC_2H_4SH	4:1	0.4	1.3	5.0	exist
f	C_3H_7SH	4:1	0.4	1.3	5.0	exist

[a] Concentration ratio between Au salt and Pt salt. [b] Quantity of Au salt used in the synthesis. [c] Byproduct was eliminated by column chromatography.

Table S2. Condition of Crystallization of a−f

cluster	ligand	good solvent	poor solvent	time
a	$SCH(CH_3)_2$	THF	methanol	3 weeks
b	$SCH_2Ph(CH_3)_3$	toluene	methanol	1 week
c	SCH_2Ph^tBu	toluene	ethanol	1 week
d	SCH_2PhCl	toluene	ethanol	1 week
e	SC_2H_4Ph	toluene	ethanol	2 days
f	SC_3H_7	toluene	ethanol	1 day

Table S3. Bond Lengths between The Adjacent Au Atoms in Individual a−f

bond [a,b]	**a** [d]	**b**	**c** [d]	**d** [d]	**e**	
					R [c]	*S* [c]
Au_1−Au_2	3.255	3.287	3.250	3.329	3.162	3.404
Au_1−Au_4	3.255	3.251	3.300	3.329	3.351	3.211
Au_2−Au_3	3.255	3.251	3.207	3.335	3.399	3.361
Au_3−Au_4	3.255	3.287	3.257	3.335	3.267	3.179

[a] See Figure S6 and S7. [b] Å. [c] Enantiomer (see Figure S16). [d] Enantiomer of these clusters have same bond lengths for both *R* and *S* enantiomers.

Table S4. Bond Lengths between Au and Pt Atoms in Individual a−f

bond [a,b]	**a** [d]	**b**	**c** [d]	**d** [d]	**e**	
					R [c]	*S* [c]
Pt_1−Au_1	3.319	3.308	3.287	3.339	3.402	3.449
Pt_1−Au_2	3.319	3.401	3.327	3.285	3.302	3.223
Pt_1−Au_3	3.319	3.335	3.353	3.281	3.400	3.273
Pt_1−Au_4	3.319	3.253	3.367	3.479	3.302	3.368
Pt_2−Au_1	3.322	3.335	3.396	3.232	3.402	3.348
Pt_2−Au_2	3.322	3.253	3.330	3.482	3.302	3.317
Pt_2−Au_3	3.322	3.308	3.290	3.385	3.400	3.257
Pt_2−Au_4	3.322	3.401	3.322	3.220	3.302	3.375

[a] See Figure S6 and S7. [b] Å. [c] Enantiomer (see Figure S16). [d] Enantiomer of these clusters have same bond lengths for both *R* and *S* enantiomers.

Table S5. Relation among 1D Structure, Chirality, Peak Splitting in XPS spectrum and Intra-Cluster Ligand Structure for a−f

cluster	ligand	1D structure [a]	enantiomer [a]	peak splitting in XPS spectrum [b]	intra-cluster ligand structure [c]
a	$SCH(CH_3)_2$	×	○	○	spread
b	$SCH_2Ph(CH_3)_3$	×	×	○	spread
c	SCH_2Ph^tBu	×	○	×	compact
d	SCH_2PhCl	○	○	×	compact
e	SC_2H_4Ph	○	○	○	spread

[a] See Figure 3. [b] See Figure S10 and S11. [c] See Figure 2.

Table S6. HOMO−LUMO and Band Gaps Obtained by Experiments and DFT Calculations for a−f

cluster	ligand	solution [a]	dried [a]	crystal [a]	DFT calc.
a	$SCH(CH_3)_2$	2.77 eV	2.88 eV	2.65 eV	−
b	$SCH_2Ph(CH_3)_3$	2.80 eV	2.69 eV	2.53 eV	−
c	SCH_2Ph^tBu	2.80 eV	2.75 eV	2.58 eV	−
d	SCH_2PhCl	2.82 eV	2.79 eV	2.62 eV	2.17 eV
e	SC_2H_4Ph	2.82 eV	2.85 eV	2.46 eV	2.17 eV

[a] See Figure S20.

4. Additional Figures

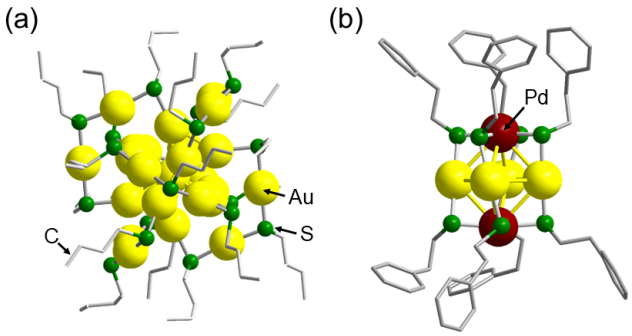

Figure S1. Geometrical structures of individual (a) $[Au_{25}(SC_4H_9)_{18}]^0$ and (b) $[Au_4Pd_2(SC_2H_4Ph)_8]^0$.[8,9]

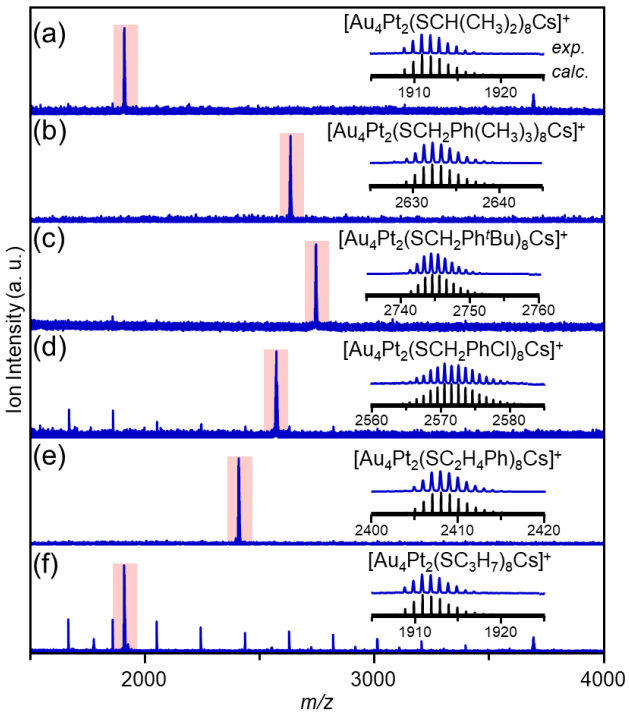

Figure S2. Positive-ion ESI mass spectra of products; $[Au_4Pt_2(SR)_8]^0$ (SR = (a) $SCH(CH_3)_2$, (b) $SCH_2Ph(CH_3)_3$, (c) SCH_2Ph^tBu, (d) SCH_2PhCl, (e) SC_2H_4Ph and (f) SC_3H_7). In this mass spectrometry, Cs^+ ion (CH_3COOCs salt) was added to the solution as the cation source.[10] In (d)(f), the peaks attributed to $[(CH_3COOCs)_xCs]^+$ also appeared together with the peak of $[Au_4Pt_2(SCH_2PhCl)_8Cs]^+$ or $[Au_4Pt_2(SC_3H_7)_8Cs]^+$.[10]

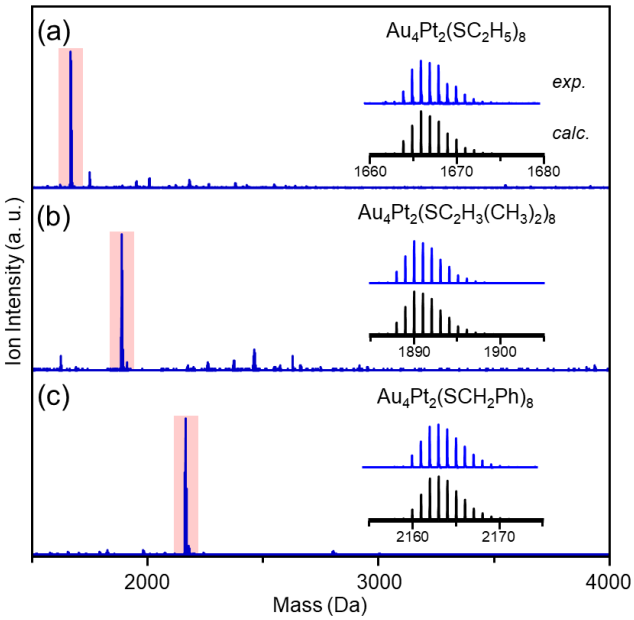

Figure S3. Positive-ion MALDI mass spectra of (a) $[Au_4Pt_2(SC_2H_5)_8]^0$, (b) $[Au_4Pt_2(SC_2H_3(CH_3)_2)_8]^0$, and (c) $[Au_4Pt_2(SCH_2Ph)_8]^0$.

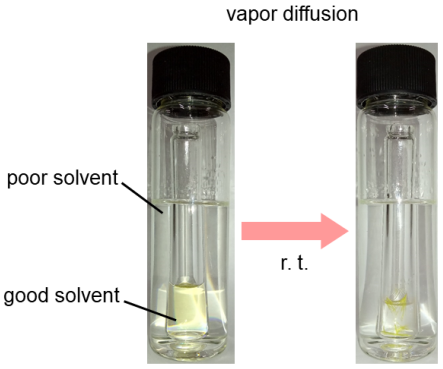

Figure S4. Crystallization method (vapor diffusion) of **a**−**f**. For the kinds of solvents, please see Table S2.

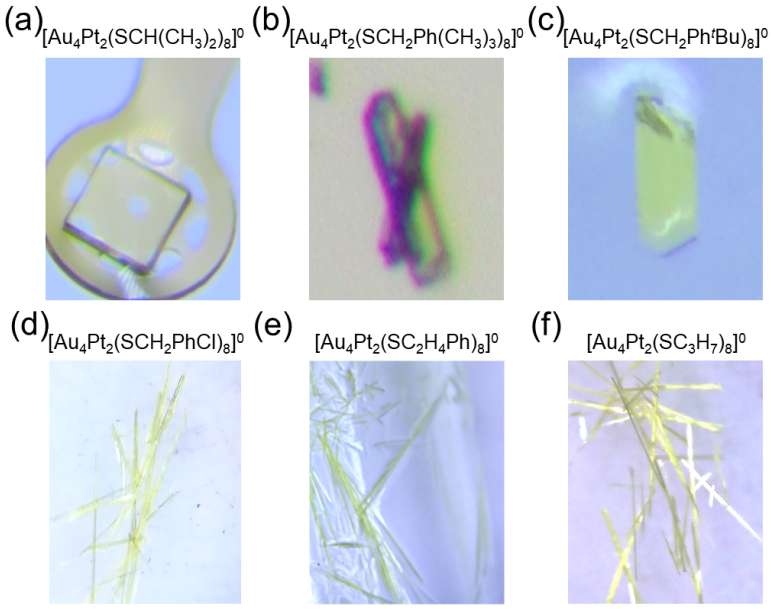

Figure S5. Photographs of crystals of products; $[Au_4Pt_2(SR)_8]^0$ (SR = (a) $SCH(CH_3)_2$, (b) $SCH_2Ph(CH_3)_3$, (c) SCH_2Ph^tBu, (d) SCH_2PhCl, (e) SC_2H_4Ph and (f) SC_3H_7).

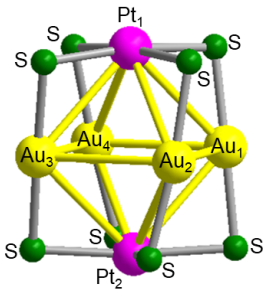

Figure S6. Numbering of Au and Pt atoms for the estimation of bond lengths (Table S3 and S4).

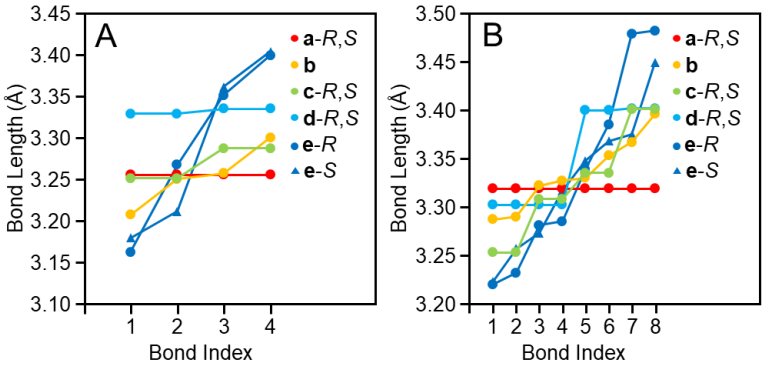

Figure S7. Bond-length distribution of (A) Au−Au and (B) Au−Pt bonds for **a**−**e** shown using bond index of Figure S6. Bond-length distribution of **e** varies depending on the enantiomer (*R* or *S*), whereas those of **a**, **c**, and **d** are same between the enantiomers (*R* and *S*) (Table S3 and S4).

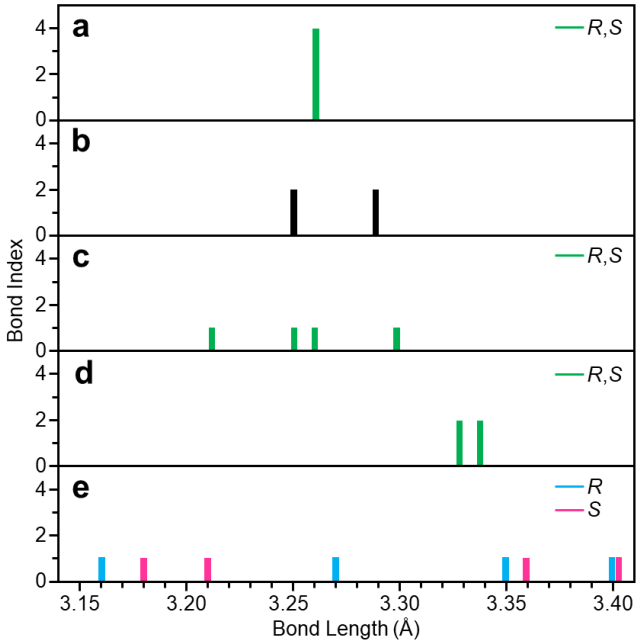

Figure S8. Bond-length distribution of Au−Au bonds for **a**−**e**. Bond-length distribution of **e** varies depending on the enantiomer (*R* or *S*), whereas those of **c** and **d** are same between the enantiomers (R and S) (Table S3 and S4).

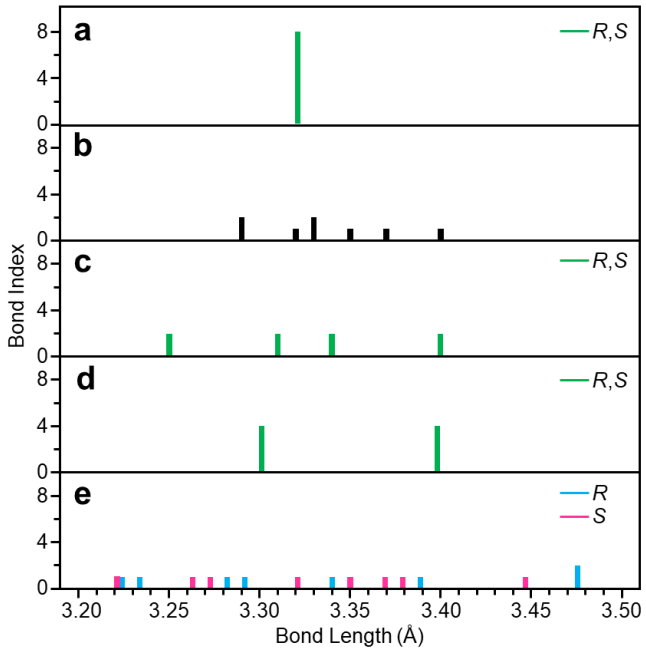

Figure S9. Bond-length distribution of Au−Pt bonds for **a**−**e**. Bond-length distribution of **c** varies depending on the enantiomer (*R* or *S*), whereas those of **c** and **d** are same between the enantiomers (R and S) (Table S3 and S4).

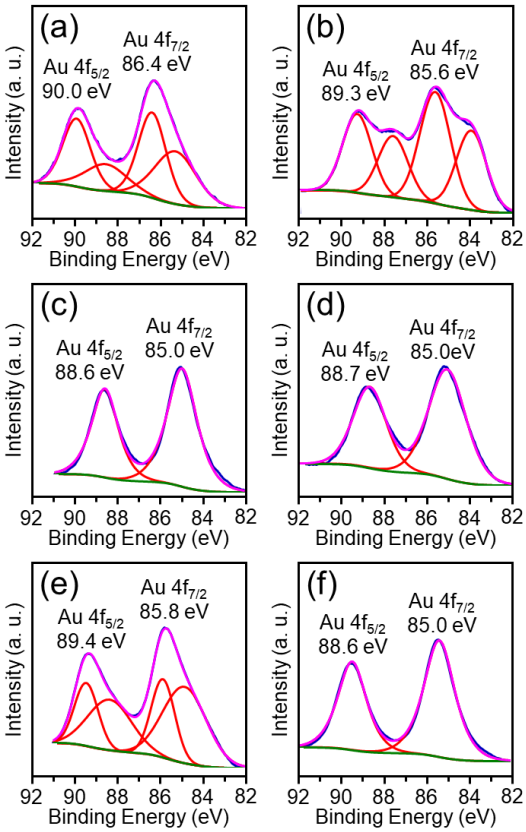

Figure S10. Au 4f spectra of **a**–**f**; $[Au_4Pt_2(SR)_8]^0$ (SR = (a) $SCH(CH_3)_2$, (b) $SCH_2Ph(CH_3)_3$, (c) SCH_2Ph^tBu, (d) SCH_2PhCl, (e) SC_2H_4Ph and (f) SC_3H_7). The observed peak positions are well consistent with those of small thiolate-protected Au clusters.[11] For **a**, **b** and **e**, Au 4f peak was fitted with two peaks, indicating that two kinds of Au atoms exist in these clusters (Table S5). In these clusters, the ligands are distributed in a comparatively isotopic manner in contract to the other clusters (**c** and **d**). Thus, the stress in the metal core, caused by the formation of this $[Au_4Pt_2(SR)_8]^0$ structure, might be a little in the metal core of this group (**a**, **b**, and **e**) compared with the cases of other clusters (**c** and **d**). This little stress might lead to the generation of the two kinds of Au and Pt atoms in these clusters.

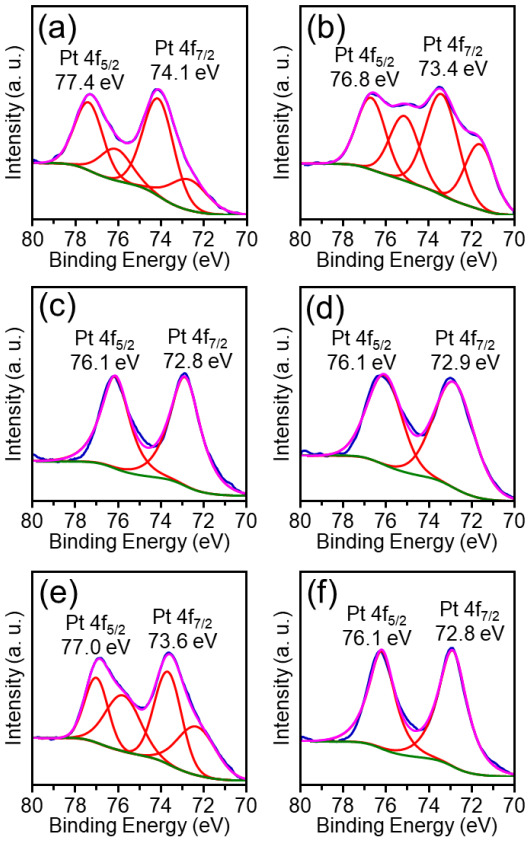

Figure S11. Pt 4f spectra of **a**–**f**; $[Au_4Pt_2(SR)_8]^0$ (SR = (a) $SCH(CH_3)_2$, (b) $SCH_2Ph(CH_3)_3$, (c) SCH_2Ph^tBu, (d) SCH_2PhCl, (e) SC_2H_4Ph and (f) SC_3H_7). For **a**, **b** and **e**, Pt 4f peak was fitted with two peaks, indicating that two kinds of Pt atoms exist in these clusters (Table S5). In these clusters, the ligands are distributed in a comparatively isotopic manner in contract to the other clusters (**c** and **d**). Thus, the stress in the metal core, caused by the formation of this $[Au_4Pt_2(SR)_8]^0$ structure, might be a little in the metal core of this group (**a**, **b**, and **e**) compared with the cases of other clusters (**c** and **d**). This little stress might lead to the generation of the two kinds of Au and Pt atoms in these clusters.

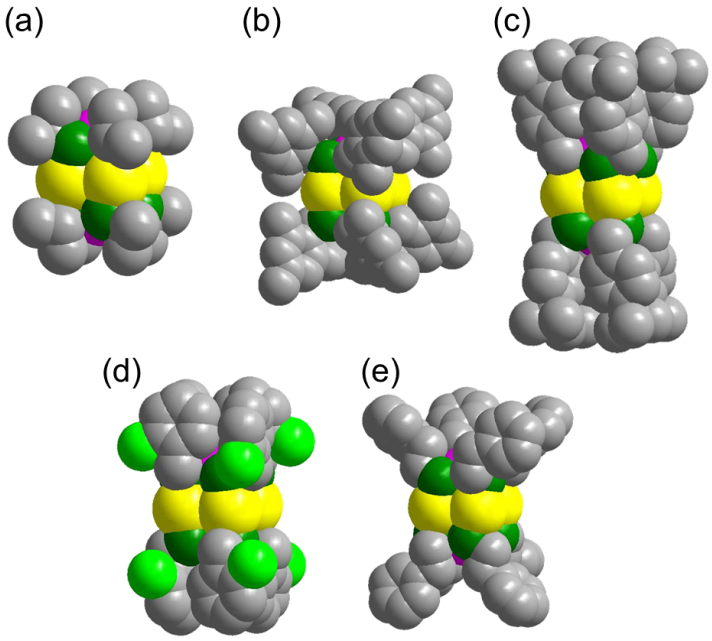

Figure S12. Geometrical structures of individual **a**–**e** shown by space filling model; $[Au_4Pt_2(SR)_8]^0$ (SR = (a) $SCH(CH_3)_2$, (b) $SCH_2Ph(CH_3)_3$, (c) SCH_2Ph^tBu, (d) SCH_2PhCl and (e) SC_2H_4Ph.

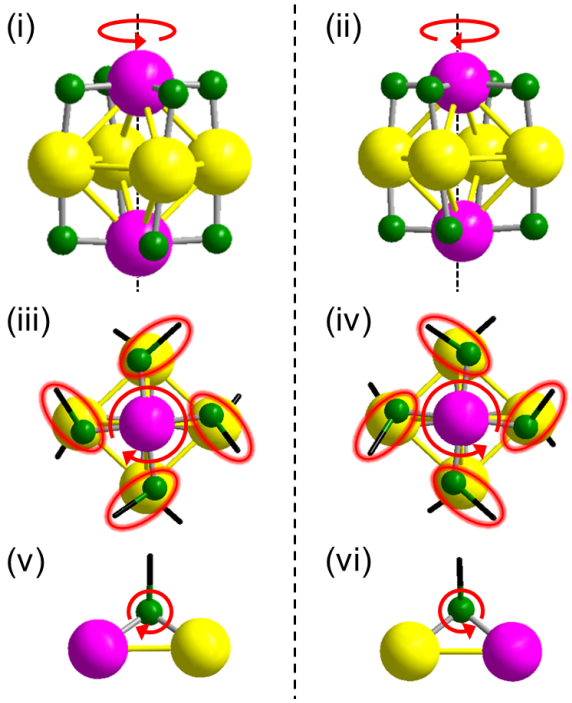

Figure S13. Enantiomer[9] observed for **a**; (i)(iii)(v) *R* enantiomer and (ii)(iv)(vi) *S* enantiomer. (i)(ii) show the side views for *R* and *S* enantiomers, and (iii)(iv) show the top views for *R* and *S* enantiomer. (v)(vi) show the chirality of sulfur for *R* and *S* enantiomer. Sulfur has four substituents composed Au, Pt, H, and lone pair electrons, producing enantiomers.

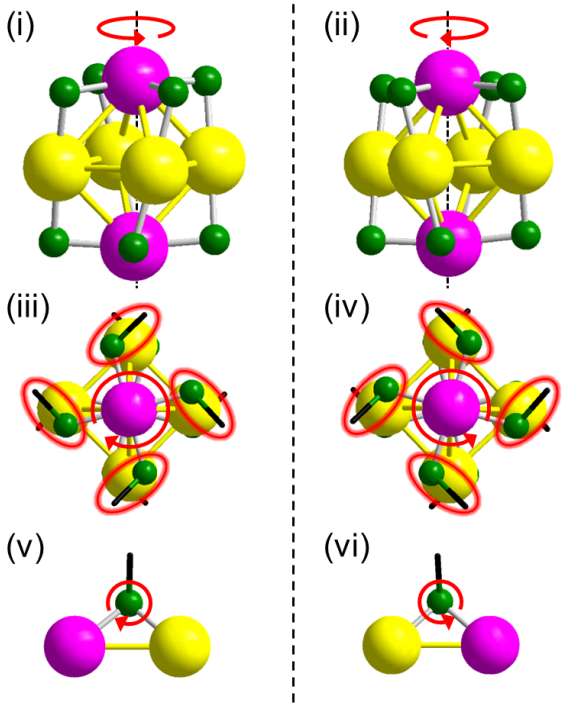

Figure S14. Enantiomer[9] observed for **c**; (i)(iii)(v) *R* enantiomer and (ii)(iv)(vi) *S* enantiomer. (i)(ii) show the side views for *R* and *S* enantiomers, and (iii)(iv) show the top views for *R* and *S* enantiomer. (v)(vi) show the chirality of sulfur for *R* and *S* enantiomer. Sulfur has four substituents composed Au, Pt, H, and lone pair electrons, producing enantiomers.

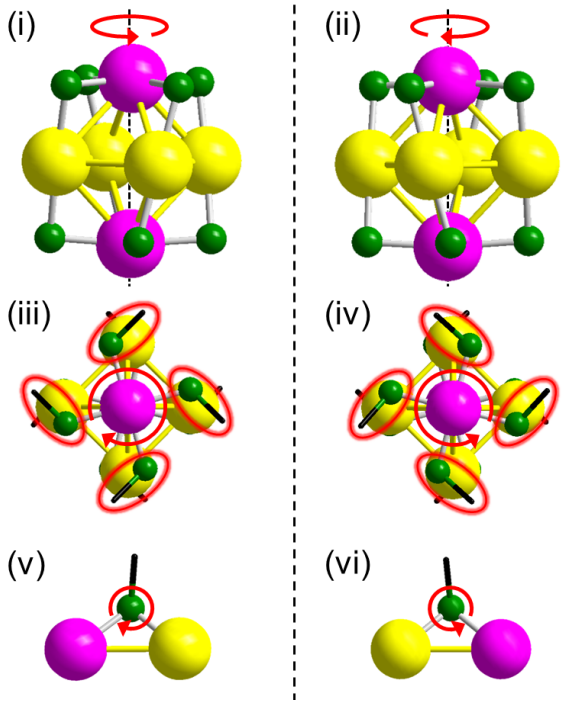

Figure S15. Enantiomer[9] observed for **d**; (i)(iii)(v) *R* enantiomer and (ii)(iv)(vi) *S* enantiomer. (i)(ii) show the side views for *R* and *S* enantiomers, and (iii)(iv) show the top views for *R* and *S* enantiomer. (v)(vi) show the chirality of sulfur for *R* and *S* enantiomer. Sulfur has four substituents composed Au, Pt, H, and lone pair electrons, producing enantiomers.

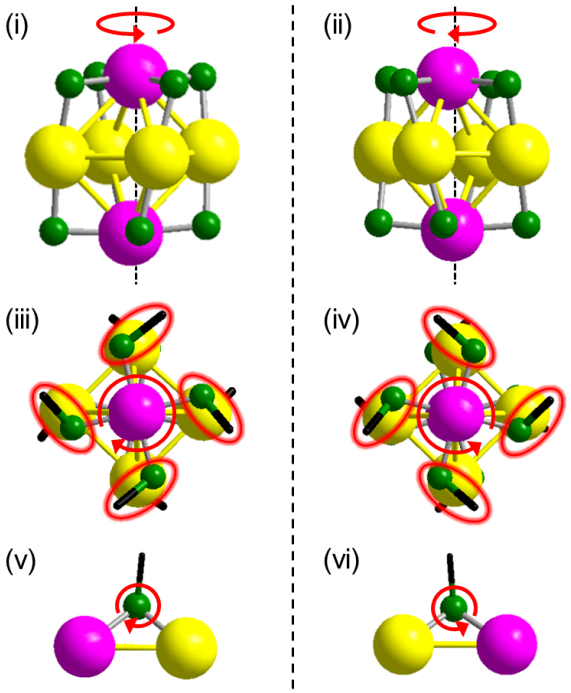

Figure S16. Enantiomer[9] observed for **e**; (i)(iii)(v) *R* enantiomer and (ii)(iv)(vi) *S* enantiomer. (i)(ii) show the side views for *R* and *S* enantiomers, and (iii)(iv) show the top views for *R* and *S* enantiomer. (v)(vi) show the chirality of sulfur for *R* and *S* enantiomer. Sulfur has four substituents composed Au, Pt, H, and lone pair electrons, producing enantiomers.

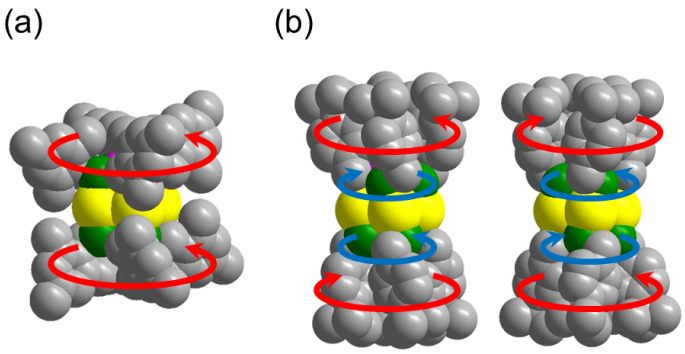

Figure S17. The way of the rotation of the core (blue circle) and the ligand layer (red circle) in (a) **b** and (b) **e** (*R* and *S*). In the case of the structure of (a), there is no enantiomers.

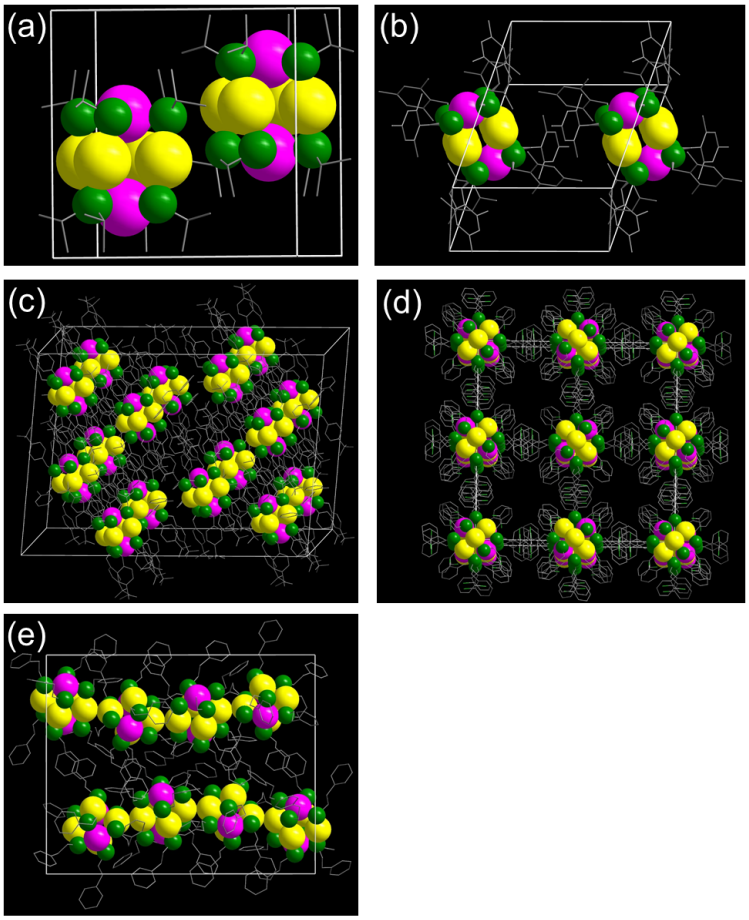

Figure S18. Unit cell of the crystal of **a**–**e**; $[Au_4Pt_2(SR)_8]^0$ (SR = (a) $SCH(CH_3)_2$, (b) $SCH_2Ph(CH_3)_3$, (c) SCH_2Ph^tBu, (d) SCH_2PhCl and (e) SC_2H_4Ph).

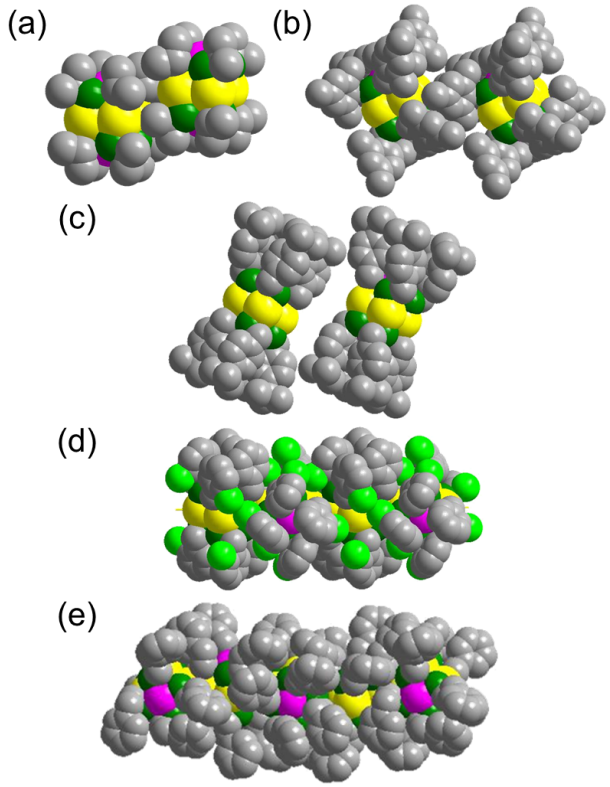

Figure S19. Relation between the adjacent clusters drawn by space filling model for **a**−**e**; $[Au_4Pt_2(SR)_8]^0$ (SR = (a) $SCH(CH_3)_2$, (b) $SCH_2Ph(CH_3)_3$, (c) SCH_2Ph^tBu, (d) SCH_2PhCl and (e) SC_2H_4Ph).

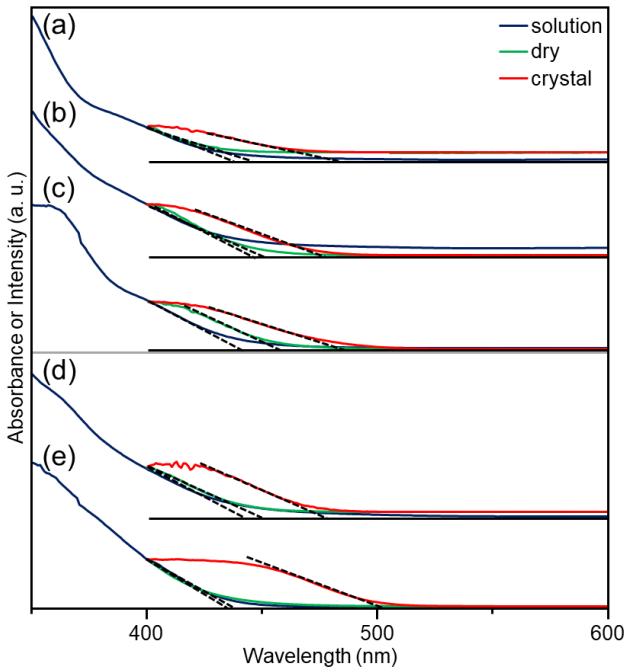

Figure S20. Estimation of the HOMO−LUMO and band gaps by extrapolating line for **a**−**e**; $[Au_4Pt_2(SR)_8]^0$ (SR = (a) $SCH(CH_3)_2$, (b) $SCH_2Ph(CH_3)_3$, (c) SCH_2Ph^tBu, (d) SCH_2PhCl and (e) SC_2H_4Ph).

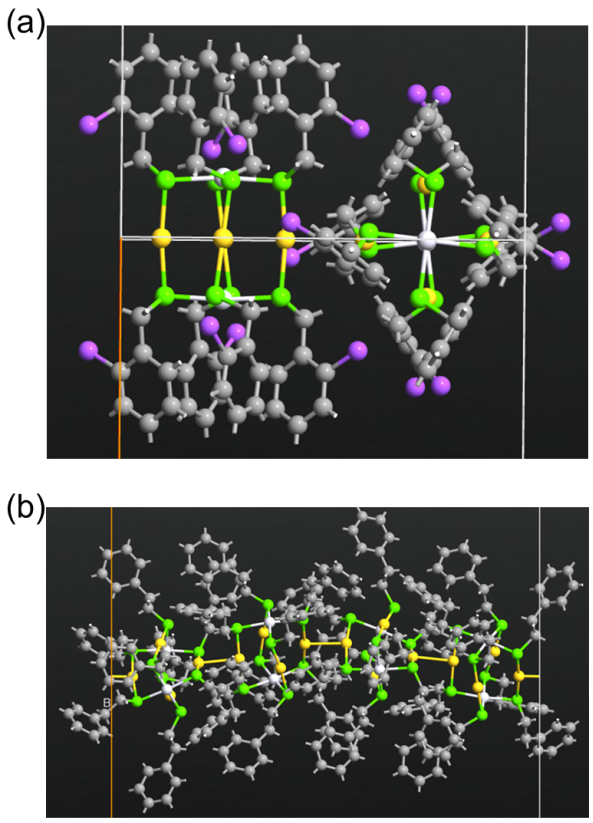

Figure S21. Geometrical structures used for DFT calculations; (a) **d** and (b) **e**. In these structures, yellow and silver bolls represent Au and Pt atoms, respectively. Green, gray, and magenta balls show S, C, and Cl atoms, respectively.

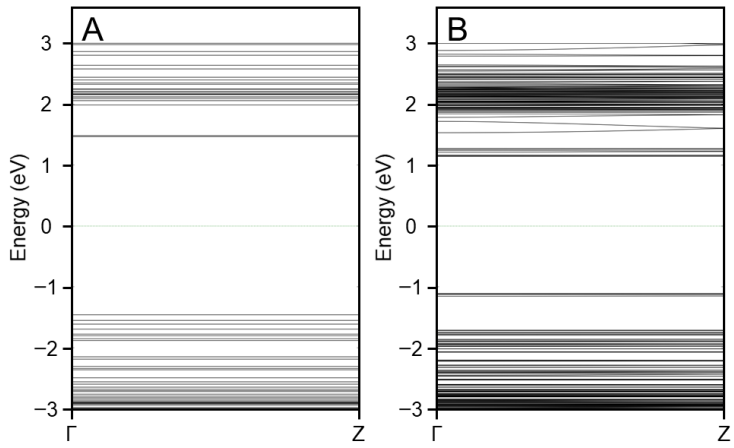

Figure S22. Calculated band structures for **e**; (A) individual cluster and (B) 1D-CS.

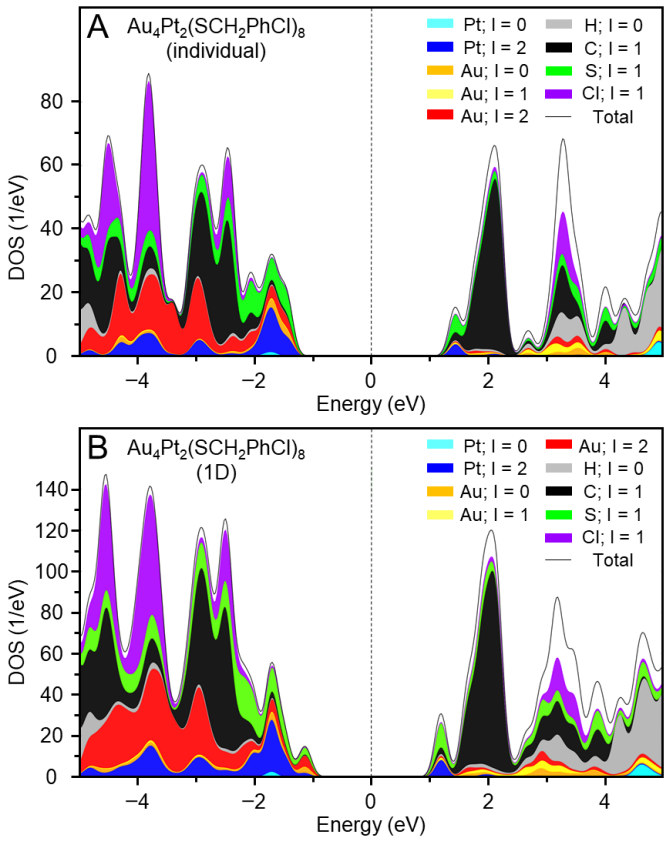

Figure S23. Projected density of states of (A) individual **d** and (B) 1D-CS of **d**.

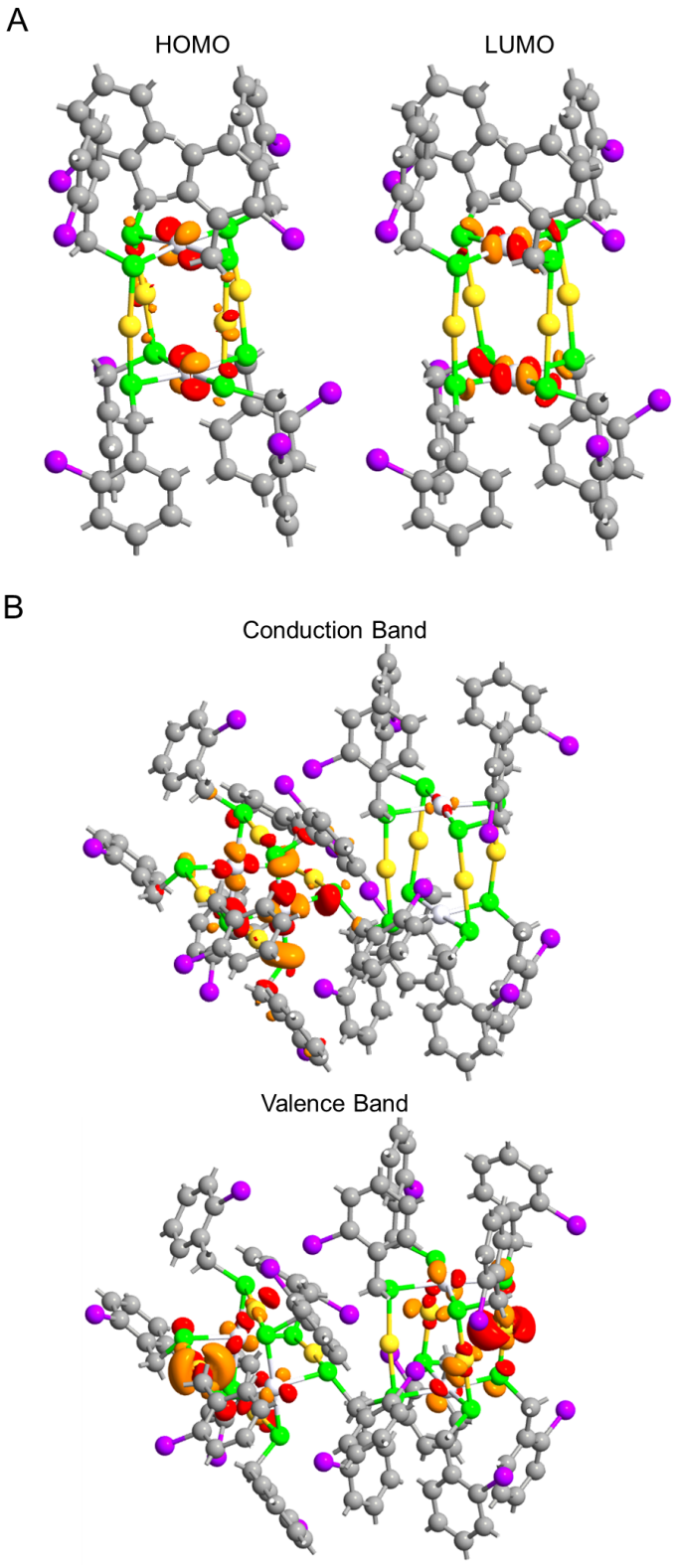

Figure S24. (A) HOMO and LUMO states of individual **d** and (B) Γ-point Bloch wave functions for conduction band minimum and valence band maximum of 1D-CS of **d**.

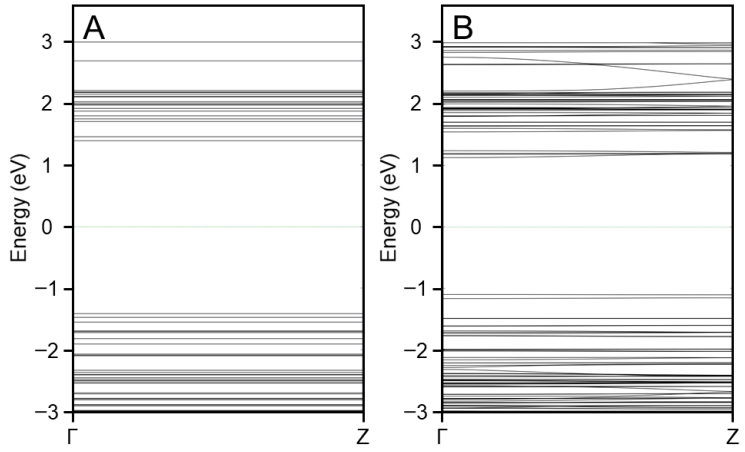

Figure S25. Calculated band structures for **d**; (A) individual cluster and (B) 1D-CS.

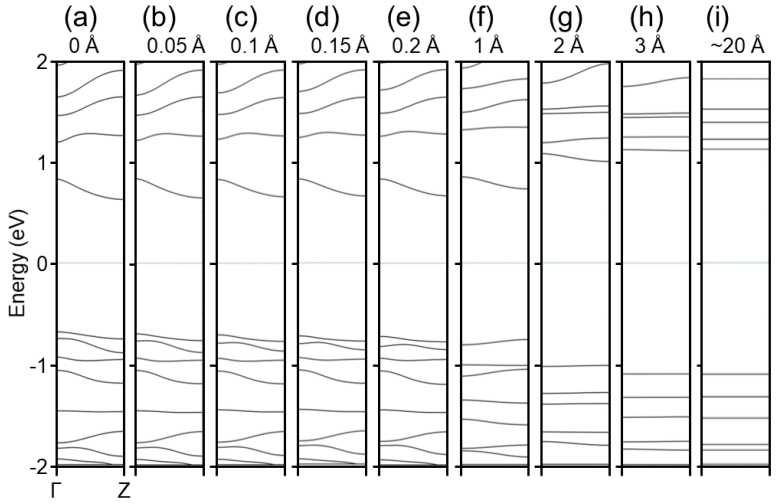

Figure S26. Band structures of $[Au_4Pt_2(SR)_8]^0$ while elongating the 1D chain using nine structures with the different inter-cluster distances. (a) the optimized inter-cluster distance (0 Å) and elongated distance from the optimized inter-cluster distance by (b) 0.05 Å, (c) 0.1 Å, (d) 0.15 Å, (e) 0.2 Å, (f) 1 Å, (g) 2 Å, (h) 3 Å, and (i) ~20 Å (individual). These results demonstrate that the band gap increases with the decrease of inter-cluster distance, namely, the expansion of band gap is caused by the decrease of inter-cluster distance.

5. Additional Information for Crystalized Clusters

5.1. Crystal Data

Crystal data and some of the important structural refinement parameters for cluster (**a**−**e**) are given below.

Cluster a: $Au_4C_{24}Pt_2S_8$; M_w. 1722.77; tetragonal, P4/n (no. 85); a= b= 12.704(2) Å, c= 12.678(2) Å, α =β= γ =90 °; V= 2046.1(7) $Å^3$; T=100(2) K; Z=2; μ(Mo Kα) = 21.517 mm^{-1}; Total reflections measured 5544 (3.212° ≤ 2Θ ≤ 46.36°) and unique reflections are 1134 unique (R_{int} = 0.0448) which were used in all calculations. Then, final *wR2* of all data was 0.1515 and *R1* was 0.0531 (I>2σ (I)).

All the details of crystal data and structural refinement parameters are tabulated in the followings.

Cluster b: $C_{80}H_{104}Au_4Pt_2S_8$; M_w. 2500.15 g/mol; triclinic, P-1 (No. 2); a= 12.5695(19) Å, b=13.435(2) Å, c=14.369(2) Å, α = 110.030(2)°, β= 107.9840(10)°, γ = 103.3310(10)°; V= 2008.9(5) $Å^3$; T=100 K; Z=1; μ (Mo K_α) =10.993 mm^{-1}; Total 20537 reflections measured (3.332° ≤ 2Θ ≤ 52.66°) and unique reflections are 8081 unique (R_{int} = 0.0268) which were used in all calculations. Then, final *wR2* of all data was 0.0631and *R1* was 0.0233 (I>2σ (I)).

Cluster c: $C_{98.5}H_{128}Au_4Pt_2S_8$; M_w. 2746.53; monoclinic, C2/c (no. 15); a= 44.070(6) Å, b= 14.7091(19) Å, c= 31.214(4) Å, β=98.553(2) °; V= 20009(4)$Å^3$; T=100(2) K; Z=8; μ(Mo Kα) = 8.839 mm^{-1}; Total reflections measured 59805 (2.638° ≤ 2Θ ≤ 58.31°) and unique reflections are 24716 unique (R_{int} = 0.0314) which were used in all calculations. Then, final *wR2* of all data was 0.0720 and *R1* was 0.0317 (I>2σ (I)).

Cluster d: $Au_4C_{56}Cl_8Pt_2S_8$; M_w. 2390.69; tetragonal, $I4_1/acd$ (no. 142); a= 29.903(7) Å, b= 29.903(7) Å, c= 15.862(4) Å, α =β= γ =90 °; V= 14183(8) $Å^3$; T=100(2) K; Z=8; μ(Mo Kα) = 12.743 mm^{-1}; Total reflections measured 16430 (3.852° ≤ 2Θ ≤ 37.772°) and unique reflections are 1411 unique (R_{int} = 0.0540) which were used in all calculations. Then, final *wR2* of all data was 0.0540 and *R1* was 0.0778 (I>2σ (I)).

Cluster e: $C_{67.5}H_{76}Au_4Pt_2S_8$; M_w. 2321.80 g/mol; monoclinic, $P2_1/n$ (No. 14); a= 18.0367(17) Å, b=30.034(3) Å, c=24.600(2) Å, β= 94.5890(10)°; V= 13284(2) $Å^3$; T=100.15 K; Z=8; μ (Mo K_α) =13.290 mm^{-1}; Total 64038 reflections measured (2.64° ≤ 2Θ ≤ 50.054°) and unique reflections are 23360 unique (R_{int} = 0.0702) which were used in all calculations. Then, final *wR2* of all data was 0.0822 and *R1* was 0.0409 (I>2σ (I)).

Table S7. Details of Crystal Data and Structural Refinement Parameters in Cluster a and b

Cluster	**a**	**b**
Empirical formula	$Au_4C_{24}Pt_2S_8$	$C_{80}H_{104}Au_4Pt_2S_8$
Formula weight	1722.77	2500.15
Temperature/K	100	100
Crystal system	tetragonal	triclinic
Space group	P4/n	P-1
a/Å	12.704(2)	12.5672(18)
b/Å	12.704(2)	13.4332(19)
c/Å	12.678(2)	14.369(2)
α/°	90	110.0380(2)
β/°	90	107.9820(10)
γ/°	90	103.3270(10)
Volume/$Å^3$	2046.1(7)	2007.8(5)
Z	2	1
ρ_{calc}g/cm^3	2.796	2.068
μ/mm^{-1}	21.517	10.999
F(000)	1488.0	1184.0
Crystal size/mm^3	0.25 × 0.15 × 0.15	0.3 × 0.15 × 0.12
Radiation MoKα	MoKα (λ = 0.71073)	MoKα (λ = 0.71073)
2Θ range for data collection/°	3.212 to 46.36	3.332 to 52.66
Index ranges	-14 ≤ h ≤ 12, -14 ≤ k ≤ 13, -14 ≤ l ≤ 10	-15 ≤ h ≤ 15, -16 ≤ k ≤ 16, -17 ≤ l ≤ 17

Reflections collected	5544	21672
Independent reflections	1134 [R_{int} = 0.0448, R_{sigma} = 0.0428]	8888 [R_{int} = 0.0273, R_{sigma} = 0.0326]
Data/restraints/ parameters	1134/340/176	8888/0/436
Goodness-of-fit on F^2	1.138	1.062
Final R indexes [I>=2σ (I)]	R_1 = 0.0531, wR_2 = 0.1483	R_1 = 0.0238, wR_2 = 0.0625
Final R indexes [all data]	R_1 = 0.0587, wR_2 = 0.1515	R_1 = 0.0263, wR_2 = 0.0638
Largest diff. peak/hole / e $Å^{-3}$	4.46/-1.55	2.44/-1.06

Table S8. Details of Crystal Data and Structural Refinement Parameters in Cluster c and d

Cluster	**c**	**d**
Empirical formula	$C_{98.5}H_{128}Au_4Pt_2S_8$	$Au_4C_{56}Cl_8Pt_2S_8$
Formula weight	2746.53	2390.69
Temperature/K	100	100
Crystal system	monoclinic	tetragonal
Space group	C2/c	$I4_1/acd$
a/Å	44.070(6)	29.903(7)
b/Å	14.7091(19)	29.903(7)
c/Å	31.214(4)	15.862(4)
α/°	90	90
β/°	98.553(2)	90
γ/°	90	90
Volume/$Å^3$	20009(4)	14183(8)
Z	8	8
$\rho_{calc}g/cm^3$	1.823	2.239
μ/mm^{-1}	8.839	12.743
F(000)	10552.0	8576.0
Crystal size/mm^3	0.2 × 0.15 × 0.12	0.12 × 0.035 × 0.03
Radiation MoKα	MoKα (λ = 0.71073)	MoKα (λ = 0.71073)
2Θ range for data collection/°	2.638 to 58.31	2.706 to 41.818
Index ranges	$-55 \le h \le 60$, $-17 \le k \le 20$, $-38 \le l \le 42$	$-25 \le h \le 30$, $-28 \le k \le 30$, $-15 \le l \le 11$
Reflections collected	59805	15010
Independent reflections	24716 [R_{int} = 0.0314, R_{sigma} = 0.0467]	1910 [R_{int} = 0.0536, R_{sigma} = 0.0406]
Data/restraints/ parameters	24716/85/1011	1910/174/154
Goodness-of-fit on F^2	1.015	1.098
Final R indexes [I>=2σ (I)]	R_1 = 0.0317, wR_2 = 0.0634	R_1 = 0.1038, wR_2 = 0.3015
Final R indexes [all data]	R_1 = 0.0586, wR_2 = 0.0720	R_1 = 0.1480, wR_2 = 0.3552
Largest diff. peak/hole / e $Å^{-3}$	1.45/-0.96	3.12/-1.67

Table S9. Details of Crystal Data and Structural Refinement Parameters in Cluster e

Cluster	**e**
Empirical formula	$C_{67.5}H_{76}Au_4Pt_2S_8$
Formula weight	2321.80
Temperature/K	100.15
Crystal system	monoclinic
Space group	$P2_1/n$
a/Å	18.0367(17)
b/Å	30.034(3)

c/Å	24.600(2)
α/°	90
β/°	94.5890(10)
γ/°	90
Volume/Å^3	13284(2)
Z	8
ρ_{calc}g/cm^3	2.322
μ/mm^{-1}	13.290
F(000)	8648.0
Crystal size/mm^3	0.3 × 0.04 × 0.04
Radiation MoKα	MoKα (λ = 0.71073)
2Θ range for data collection/°	2.64 to 50.054
Index ranges	-21 ≤ h ≤ 20, -35 ≤ k ≤ 33, -29 ≤ l ≤ 16
Reflections collected	64038
Independent reflections	23360 [R_{int} = 0.0702, R_{sigma} = 0.0902]
Data/restraints/ parameters	23360/1713/1469
Goodness-of-fit on F^2	0.994
Final R indexes [I>=2σ (I)]	R_1 = 0.0409, wR_2 = 0.0705
Final R indexes [all data]	R_1 = 0.0818, wR_2 = 0.0822
Largest diff. peak/hole / e Å^{-3}	1.21/-1.78

5.2. Structure Quality Indicators and Refinement Details

First initial model of each structure of all the clusters containing heavy atoms (metal and sulfur) and few carbon atoms of thiolates were solved by Shelxt using intrinsic phasing method.[3] Total structures of all the clusters were refined by full-matrix least-squares method against F^2 by SHELXL-2018/3[4] using Olex2 software.[5] Electron density corresponding to disordered solvent molecule of cluster **e** was SQUEEZED by PLATON[12] in Olex2 platform (Details is appended in cif file). Cluster **a** has positional disorder in its structure which was refined using PART command in SHELXL 2018/3 and ratio of PARTS is 0.89/0.11. Some high Q peaks appearing inside near to cluster cores are due to similar positional disorder which, however, could not be refined due to very low electron density (~4 for metal positions). Diffraction data of cluster **d** lack higher angle data (resolution below 1.1 Å) which were collected at very high exposure time (360 sec.). Even after repeated attempt, we could not get diffraction data having higher angle data for the same cluster. Except cluster **a** and **d**, the hydrogen atoms were placed at calculated positions with the exception of disordered H atoms, and their positions were refined with a riding model. During overall refinement, several restrain and constrain (ISOR, RIGU, SIMU, DFIX, AFIX 66 and EADP) have been used.

6. References

1. A. Dass, A. Stevenson, G. R. Dubay, J. B. Tracy and R. W. Murray, *J. Am. Chem. Soc.*, 2008, **130**, 5940–5946.
2. APEX III software suite, Bruker-AXS, 2016.
3. G. M. Sheldrick, *Acta Cryst.*, 2015, **A71**, 3–8.
4. G. M. Sheldrick, *Acta Cryst.*, 2015, **C71**, 3–8.
5. O. V. Dolomanov, L. J. Bourhis, R. J. Gildea, J. A. K. Howard and H. Puschmann, *J. Appl. Cryst.*, 2009, **42**, 339–341.
6. M. Brandbyge, J.-L. Mozos, P. Ordejón, J. Taylor and K. Stokbro, *Phys. Rev. B*, 2002, **65**, 165401.
7. J. Taylor, H. Guo and J. Wang, *Phys. Rev. B,* 2001, **63**, 245407.
8. M. D. Nardi, S. Antonello, D.-e. Jiang, F. Pan, K. Rissanen, M. Ruzzi, A. Venzo, A. Zoleo and F. Maran, *ACS Nano*, 2014, **8**, 8505–8512.
9. J. Chen, L. Liu, X. Liu, L. Liao, S. Zhuang, S. Zhou, J. Yang and Z. Wu, *Chem. Eur. J.*, 2017, **23**, 18187–18192.
10. H. Qian, Y. Zhu and R. Jin, *Proc. Natl. Acad. Sci. USA,* 2012, **109**, 696–700.
11. Y. Negishi, K. Nobusada, T. Tsukuda, *J. Am. Chem. Soc.*, 2005, **127**, 5261–5270.
12. A. L. Spek, *Acta Cryst.*, 2015, **C71**, 9–18.